Acta Materialia 286 (2025) 120753

Contents lists available at ScienceDirect

Acta Materialia

journal homepage: www.elsevier.com/locate/actamat

Full length article

Plasticity of metallic glasses dictated by their state at the fragile-to-strong transition temperature

Achraf Atila *, Sergey V. Sukhomlinov, Marc J. Honecker, Martin H. Müser

Department of Material Science and Engineering, Saarland University, Saarbrücken, 66123, Germany

ARTICLE INFO

Keywords:
Bulk metallic glasses
Deformation behavior
Shear bands
Fragile-to-strong transition
Atomistic simulations

ABSTRACT

The effect of cooling on the plasticity of glasses in general, and bulk metallic glasses (BMGs) in particular, is usually studied with continuously varying cooling rates; slower cooling rates lead to stiffer, harder, and more brittle glasses than higher cooling rates. These protocols obscure any potential discontinuity that a glass might experience, depending on whether its microstructure resembles that of a fragile or a strong glass-forming liquid. Here, we use large-scale molecular dynamics to simulate the nanoindentation behavior of model BMGs ($Zr_{0.6}Cu_{0.3}Al_{0.1}$) obtained by rapidly quenching equilibrium melts from temperatures above and below the fragile-to-strong transition temperature T_{fst}, leading to fragile and strong glasses, respectively. While the contact modulus deduced from the indentation simulation evolves smoothly with the temperature T_q from which the equilibrium melt is quenched, the plastic response changes quasi-discontinuously as T_q passes through T_{fst}. In particular, strong glasses develop highly asymmetric flow profiles with mature shear bands, unlike fragile glasses. Differences are most evident in the von Mises strain localization parameter, which, after shear-band formation, takes similar values for all fragile samples and distinct values for strong samples. Moreover, seemingly erratic flow profiles for our indentation geometry produced surprisingly reproducible and, thus, deterministic features. It remains to be determined to what extent other classes of glass formers follow our observation that plastic behavior is significantly influenced by whether the melt is fragile or strong when it falls out of equilibrium during cooling.

1. Introduction

Bulk metallic glasses (BMGs) have elastic strain limits of up to 5% [1] and high tensile [2] as well as yield [3] strengths of order 1 GPa exceeding that of crystalline and poly-crystalline metals by an order of magnitude. At the same time, BMGs have defied the rule that materials cannot be simultaneously strong and tough [3]. In fact, BMGs are known to have the highest known damage tolerance [3], which is the product of fracture yield strength and toughness. On the downside, BMGs generally strain soften, making them prone to localized deformations in the form of shear bands [4–7], whereby undesirable surface markings can be produced, which ultimately evolve into cracks. This contrasts conventional metals, which usually strain harden, because dislocations are the main carriers of plasticity [8,9]. This behavior of BMGs limits the moldability of most BMGs and their widespread technological applicability.

One subject of ongoing research is how the thermal history of a BMG affects its atomic structure [10] and, thereby, its deformation mechanisms, most notably shear bands [4,11,12]. It is established both experimentally [13] and from simulations [14,15] that BMGs produced with a small cooling rate are stronger but also more prone to shear banding and thereby to brittle behavior [16] than those quenched more quickly. In contrast, silica-based oxide glasses are brittle. A distinguishing feature of silica-based glasses is the ratio of the fragile-to-strong transition (FST) temperature T_{fst} and the glass transition temperature T_g, i.e., typical values of T_{fst}/T_g exceed unity for silicates but are of order unity for BMGs. This prompts us to hypothesize that the brittleness of a glass is significantly influenced by the degree to which its atomic structure resembles that of a strong or fragile melt. In particular, the question arises whether the quasi-discontinuity of both dynamic and static properties of the melt at the FST translates into discontinuities in the mechanical properties of the corresponding glass.

A few notes on the FST, which has been argued to occur in any glass-forming melt [17], and the glass transition itself may be in place. The equilibrium viscosity and atomic diffusion coefficients cross over from a non-Arrhenius to an Arrhenius dependence upon cooling in a relatively narrow temperature window near T_{fst}, which is accompanied by a breakdown of the Stokes-Einstein relation below T_{fst} [18,19]. The specific heat of melts c_p at $T > T_{fst}$ is substantially above that

* Corresponding author.
E-mail address: achraf.atila@uni-saarland.de (A. Atila).

https://doi.org/10.1016/j.actamat.2025.120753
Received 1 August 2024; Received in revised form 11 December 2024; Accepted 15 January 2025
Available online 23 January 2025

associated with the rule of Dulong-Petit. This means that structural rearrangements go beyond quasi-harmonic vibrations so that the melt is called thermodynamically *fragile*. After passing through a maximum near T_{fst} upon cooling, c_p quickly decreases to values satisfying Dulong-Petit. This is indicative of vibrations around barely changing reference structures. The melt is called *strong*. The potentially most localized abrupt change at the FST is the jump of the correlation length describing the asymptotic decay of density oscillation [20,21]. In contrast to the FST, the glass transition refers to a more continuous process in which a melt falls out of equilibrium during cooling, however, with a strong dependence on the cooling rate. Similar to the FST, the glass transition leads to a reduction of the specific heat towards the rule of Dulong-Petit.

Ascertaining to what degree FST discontinuities translate into corresponding features in the glass requires *equilibrium* melts to be quenched instantly from both above and below T_{fst} to well below T_g in the first step. This way, the glass represents the frozen-in structure of a fragile and strong melt, respectively, and hence could be called either fragile or strong glass. Whenever T_g and T_{fst} are not separated, conventional cooling protocols using constant cooling rates plus potentially holding periods below T_g generally produce a mix of fragile and strong glass, since the melt would not be fully equilibrated at $T > T_{fst}$, while some low-temperature relaxations would occur at $T < T_{fst}$. The lower the cooling rate $\dot{q}$, the more the structure leans towards a strong glass, but changes are continuous in $\dot{q}$. Thus, previous studies [15,22,23] reveal that the failure mechanisms evolve smoothly from being homogeneous in a high-$\dot{q}$ sample to localized shear bands using low $\dot{q}$ do not contradict our hypothesis that the plasticity of a bulk metallic glass might be dictated by its state at the FST.

In the remainder of this work, we use molecular dynamics (MD) simulations to contrast the mechanical behavior of strong and fragile glasses during nanoindentation. To this end, we recycle previously produced atomistic equilibrium configurations of an *in-silico* model for a ternary BMG, $Zr_{0.6}Cu_{0.3}Al_{0.1}$, which had been shown to undergo an FST in thermal equilibrium [21]. MD is an ideal tool for this study, because equilibrium melts can be quenched extremely quickly and homogeneously, preventing temperature-gradient-induced heterogeneities or residual stresses from occurring.

2. Methods

2.1. Samples preparation

In this work, we simulate the ternary alloy $Zr_{0.6}Cu_{0.3}Al_{0.1}$ using an embedded-atom potential [24] parameterized by Cheng, Ma, and Sheng [25]. This system revealed a transition from a fragile to a strong liquid at $T_{fst} \approx 830$ K [21], at which the correlation length of the long-range density fluctuations changed quasi-discontinuously by roughly 10% in a very narrow temperature range similarly as in a related experimental BMG called Vitleroy 106a [20]. Upon further cooling with a rate of about 10^7 K/s, the system fell out of equilibrium near $T_g = 747$ K.

Initial configurations were taken from the above-mentioned previous work [21], in which a sample containing about 8800 atoms was equilibrated at various temperatures, including a narrow temperature regime below T_{fst}. Thermal equilibrium had been ensured as follows: Simulations were run until the potential-energy autocorrelation function stabilized across successive runs, allowing the energy autocorrelation time τ to be estimated. It was then ensured that the combined run time at a temperature was at least 100 τ. The so-ensuing full equilibration times used during step-wise cooling were: 30 ns at $T = 1,000$ K, 64 ns at 900 K, 400 ns at 850 K, 1.25 μs at 812 K, 2.5 μs at 800 K, and 4.0 μs at 787 K. In the following, samples obtained by quenching an equilibrium sample from $T < T_{fst}$ will be referred to as *strong* glasses, while those obtained from equilibrium simulations at $T > T_{fst}$ will be called *fragile* glasses. All samples were duplicated $n_x = 3, n_y = 3, n_z = 3$ times in x, y, and z-direction, respectively, equilibrated for 4 ns at the temperature from which they were obtained, and subsequently quenched to room temperature $T = 300$ K with a cooling rate of 1 K/ps [26,27], and annealed for another 4 ns. During these simulations, a timestep of 2 fs was used with periodic boundary conditions applied to all box directions. Such equilibrated samples were replicated again to obtain a larger sample of dimension 230×16.5×86 nm^3 containing approximately 18 mio atoms. The default surface was created along the z-axis. A 1 nm thick layer of atoms at the bottom of the simulation box along the z-direction was fixed. The samples were periodic along the x- and y-direction. Next, the samples were further equilibrated for 200 ps at room temperature and 0 MPa using a timestep of 2 fs. The temperature was maintained using a Langevin thermostat [28] while the pressure was controlled using Nosé-Hoover chain barostat [29]. All simulations were conducted using the LAMMPS simulation package [30]. The snapshots were prepared using OVITO [31]. Additional simulations were run, in which the small, original configurations were rotated by 90° so that the old x-axis or old y-axis turned into the new z axis. Next, all replication and post-equilibration procedures were repeated as described above, which allowed us to conduct a disorder average.

2.2. Nanoindentation simulations

The indentation was performed with a rigid cylindrical indenter exerting a force of magnitude $F(r) = -K(r - R)^2$ on each atom, where K is the force constant, which we chose to be $K = 10$ eV/Å^2, r is the distance from the center of the indenter to the respective atom, and R is the radius of the indenter which was fixed to $R = 100$ nm. Lilleodden et al. [32] studied the response of single-crystalline gold to nanoindentation while varying the force constant of the indenter and found that the force–displacement curves are unaffected by the change of K. Displacement-controlled nanoindentation simulations were performed by displacing the indenter along the z-direction towards the sample with a fixed velocity of $v_i = 5$ m/s until reaching a depth of 20 nm and using a timestep of 2 fs.

2.3. Local strain analysis

The shear bands were detected using the von Mises shear strain. The von Mises strain was calculated using an affine transformation matrix to the relative neighbors through a least-square fitting [33]. The undeformed glass was chosen as a reference configuration. More details of the strain calculation can be found in Refs. [31,33]. To identify the regions with a nonaffine displacement, the current atomic configuration needs to be compared with a reference configuration. The neighbors of each particle are found by defining a sampling radius, i.e., 10 Å in our case. The local strain is then calculated from the displacements of the neighboring particles to the central one and the relative displacements that they would have if they were in a region of uniform strain. The final value of the nonaffine displacement was divided by the number of atoms within that spherical region of the same radius. More details about the calculation of the nonaffine displacements are given in Ref. [34].

2.4. Image analysis

Snapshots of the local von Mises shear strain taken at different depths during the nanoindentation process were image analyzed. To this end, pre-trained DINOv2 neural networks [35] were used for feature extraction, because DINOv2 is known for its robustness in capturing image features through self-supervised learning. The DINOv2 architecture is based on the so-called vision transformer (ViT) [36], which is currently the *de-facto* standard for computer vision. In this work, we mainly use the bare backbones ViTb/14_reg with registers [37] and ViTg/14 without registers available at GitHub (https:

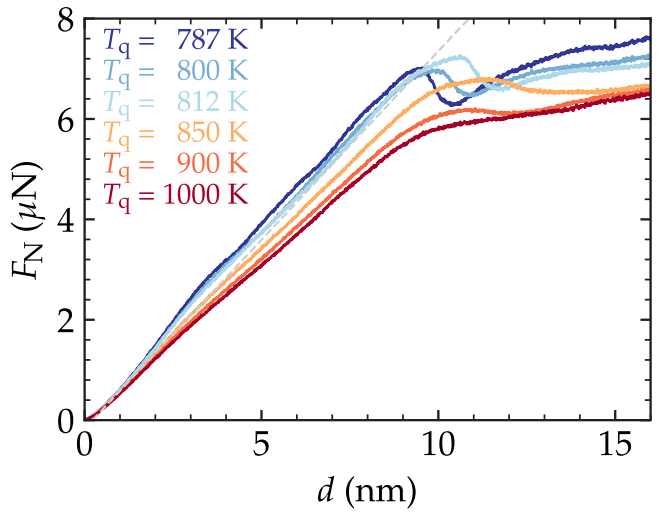

Fig. 1. Force–displacement curves during loading at $T = 300$ K and using an indentation velocity of 5 m/s. The dashed line reflects an indentation with a contact modulus of $E^* = 57.9$ GPa. Deviations of the data from linearity at very small d are due to an effectively finite-range repulsion between indenter and samples.

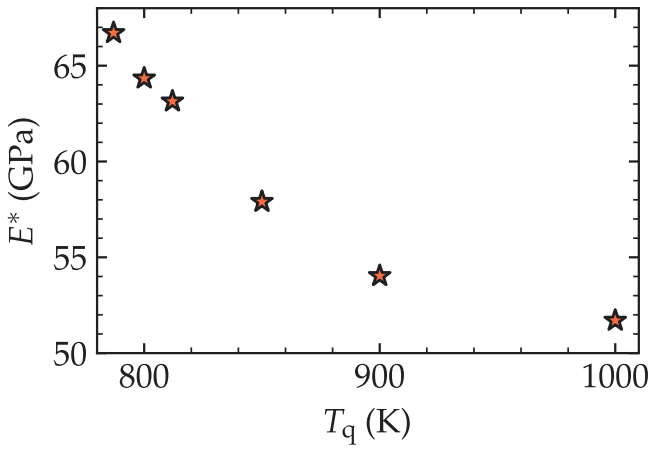

Fig. 2. Contact modulus E^* at $T = 300$ K as a function of T_q as deduced from the initial ($0.2 < d/\text{nm} < 2.5$) linear $F_N(d)$ dependence of the indentation process using $F_N(d) \approx \frac{\pi}{4} E^* L d$. The very initial $d < 0.2$ nm domain is excluded from the fit, because the finite stiffness of the cylinder-BMG repulsion causes a parabolic dependence at these extremely small indentation depths.

//github.com/facebookresearch/dinov2), because they showed the best results for our analysis. The models had been pre-trained on 142 million images in a contrastive learning setting, which allowed them to capture robust image features, although the images supposedly did not show shear bands or flow lines.

Each image was preprocessed to meet the input requirements of the DINOv2 model. The preprocessing steps included resizing the image to 224 × 224 pixels, converting it to a PyTorch [38] tensor, and applying the DINOv2-specific preprocessing function. The latter includes normalizing the images by the mean and standard deviation values of ImageNet [39] statistics: mean = [0.485, 0.456, 0.406] and standard deviation = [0.229, 0.224, 0.225]. After processing all images using the model, the cosine similarity of each pair of images was computed. It ranges from −1 (antiparallel, minimum similarity) to 1 (parallel, maximum similarity).

3. Results

In this work, we simulate the indentation process of glasses obtained from quenching equilibrium melts from six temperatures T_q to $T = 300$ K, where all indentation simulations were conducted. Three of the initial temperatures, that is, $T_1 = 787$ K, $T_2 = 800$ K, and $T_3 = 812$ K were below the fragile-to-strong cross-over temperature $T_{\text{fst}} = 830$ K, the remaining ones $T_4 = 850$ K, $T_5 = 900$ K, and $T_6 = 1{,}000$ K were above T_{fst}. Even the sample quenched from T_1 has reached equilibrium at T_1: The relaxation time of energy fluctuations in the α-relaxation regime can be estimated to be $\tau = 10$ ns and the Kohlrausch exponent to $\beta = 0.73$ [40], which yields a factor of $\exp(-(t_{\text{sim}}/\tau)^\beta) \approx 3.5 \cdot 10^{-35}$ after 4.0 μs relaxation. The density is even better relaxed than the energy since for this quantity $\tau = 1$ ns and $\beta = 0.79$ [40].

At first glance, all six samples show qualitatively similar force–displacement curves as revealed in Fig. 1: an initial Hertzian regime up to an indentation of $d \approx 2$ nm, followed by a non-elastic regime. A maximum indentation force of $F \approx 7 \pm 0.5$ μN is reached at $d \approx 10 \pm 1$ nm for all $T_q \leq 900$ K samples. After a short drop, F increases again at $d \approx 12 \pm 2$ nm.

Closer inspection of Fig. 1 reveals qualitative differences between fragile and strong glasses. All strong samples have similar $F_N(d)$ relations at $d < d_{\max}$, where $d_{\max}$ is the depth at which the force is a local maximum. In contrast, $F_N(d)$ of fragile samples reveal some T_q dependence at $d < d_{\max}$. The situation reverts when d exceeds $d_{\max}$ by a few nanometers. This time, $F_N(d)$ converges to a single dependence for all fragile glasses but reveals a weak T_q dependence for the strong glasses. Moreover, the drop in the indentation force after reaching its maximum is noticeably more pronounced for strong than for fragile glasses. This implies that the strong glasses work soften substantially more than the fragile glasses.

Subtle qualitative differences between the fragile and the strong glasses can already be noticed at a relatively small indentation depth. The strong glass starts to deviate from their linear response by assuming a left-curved $F_N(d)$ relation, while the fragile glasses adopt a minor right-curved $F_N(d)$ dependence. In contrast, the contact modulus $E^*(T_q)$ has a smooth dependence on T_q without detectable signs of a discontinuity of the function itself or its derivative, as is revealed in Fig. 2 These findings align with the existing literature, which also reports more significant effects of cooling rate on plastic than on elastic properties [15].

Despite subtle differences between fragile and strong plasticity at the early loading stages, effects are more pronounced at large indentation. To analyze plasticity, we investigated the local von Mises local shear strain, as described in Section 2. Exemplary results are shown in Fig. 3 with representatives corresponding to the three different plasticity regimes of the $F(d)$ curve, i.e., before, near, and after the maximum indentation force. Fig. S1 depicts more snapshots of the von Mises strain, i.e., for all six samples at seven depths, including one snapshot taken in the elastic regime. We also note that visualization of the shear bands using non-affine displacement squared, defined similarly as by Falk and Langer [34] but normalized to the number of neighbors, produced snapshots, which closely resembled those based on the von Mises strain, as is evidenced in Fig. S2.

Shear bands, which are the main carrier of plasticity in BMGs [6,41–43] start to occur once $F(d)$ deviates from the elastic response. They mature, i.e., the shear bands reach a stage where their growth slows down or stops after $F(d)$ reaches its maximum, at which point they have hit the surface. Contrary to previous simulations [4,15,43–45] and our fragile glasses, the *strong* samples develop visible, radially shaped shear bands with an average width of $w \approx 8$ nm. This is on par with $w \approx 10$ nm [42,46,47], which is the intrinsic thickness of mature shear bands in *ex-silico* BMGs. The shear bands of strong glasses are more localized and more asymmetric than in fragile glasses, to the extent that they could be said to differ qualitatively.

Going beyond a visual inspection of the shear bands requires a quantitative analysis to be conducted. To this end, we study the standard deviation of the atomic von Mises strain divided by its average value,

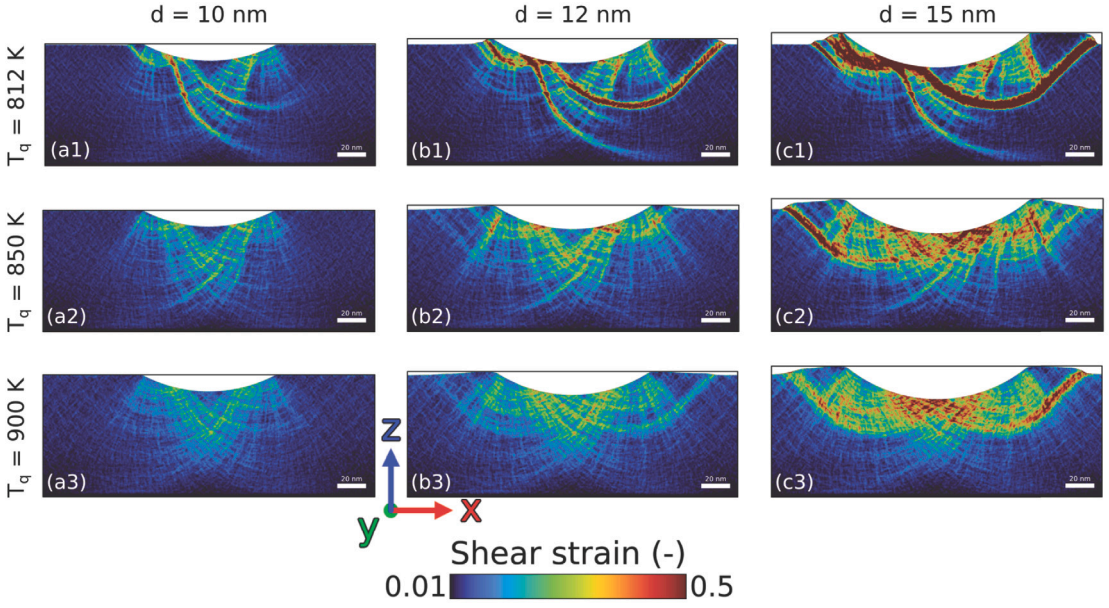

Fig. 3. Local shear strain maps for the strong and fragile glasses loaded to an indentation depth of (a) $d = 10$ nm, (b) $d = 12$ nm, and (c) $d = 15$ nm.

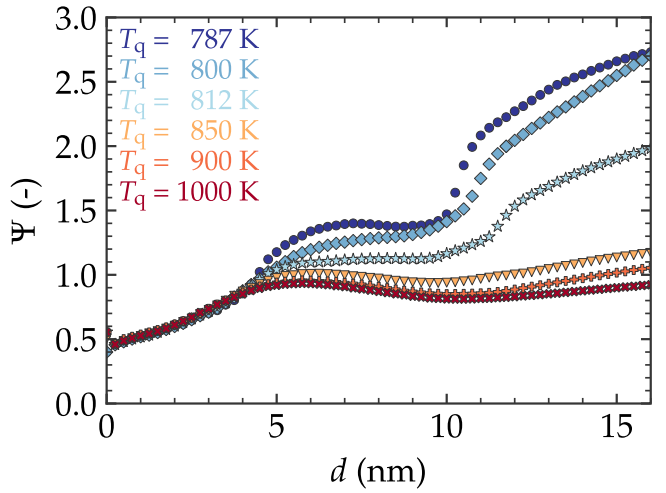

Fig. 4. Strain localization parameter Ψ as a function of the indentation depth d for the strong and fragile glasses. Different symbols are used for their respective temperatures T_q: circles for 787 K, diamonds for 800 K, stars for 812 K, triangles down for 850 K, pluses for 900 K, and crosses for 1000 K.

$\Psi = \langle \Delta\eta_n^2 \rangle^{1/2} / \langle \eta_n \rangle$, where η_n is the von Mises strain projected to atom n, $\langle ... \rangle$ an average over all atoms, and $\Delta\eta_n = \eta_n - \langle \eta_n \rangle$. Ψ is similar to a previously defined localization parameter [48] but normalized so that it does not change when atoms with zero von Mises strain are added. Like the previous parameter, Ψ is sensitive to localization because atoms with large variance tend to cluster. Results for Ψ are shown in Fig. 4. At very small d, the value for Ψ is essentially identical for all samples. This can be understood from the fact that elastic deformation is scale-invariant and, thereby, the value for Ψ at $d = 0.5$ nm is merely 2% between the most fragile and the strongest sample compared to a 25% difference in E^*.

The values of $\Psi(d)$ bifurcate at a depth of $d \gtrsim 4$ nm, where $\Psi(d)$ keeps increasing for the strong samples while they saturate otherwise. An even stronger qualitative difference between strong and fragile samples becomes apparent at $d \gtrsim 9$ nm, where the slope of $\Psi(d)$ suddenly increases near the point of the local $F_N(d)$ minima for the strong samples. At the same time, $\Psi(d)$ has no such discontinuity in the fragile samples.

From the results shown, a qualitative difference in the deformation behavior of glasses reflecting the structure of a fragile and a strong melt has become apparent. To ensure that these differences are not merely a kinetic effect resulting from the ratio of the indentation rate and the relaxation time at T_q surpassing some critical value, we performed another indentation simulation of the $T_q = 850$ K sample, however, using a ten-fold increased indentation velocity. This exceeds the ratio of relaxation times between the "strongest" (lowest T_q) and the "most fragile" (highest T_q) melt for both energy and volume relaxation.

The ten-fold increased indentation velocity produced a noticeable increase in the $F_N(d)$ relationship. However, the higher indentation velocity produces noticeably more symmetric and less localized shear bands or rather flow patterns, as is revealed in Fig. 5 both visually but also in terms of the strain-localization parameter. The higher symmetry of the flow images at the higher velocity could be argued to arise from the reduced time for an initial local symmetry breaking to migrate from small to large scales. In our simulations, the symmetry breaking arises due to structural heterogeneities, potentially to some degree also by thermal fluctuations.

To explore the degree to which our findings can be tested experimentally if images of flow profiles are available but there is no spatially resolved von Mises strain, we quantified the similarity between the shear-band signature using two different models, as described in the Methods section. The result produced with ViT_g/14 is shown in Fig. 6. At each indentation depth, inspection of both colors and numbers included in the figure generally gives the largest difference in similarity between the hottest strong and coolest fragile samples. This claim holds for both models. Moreover, the ViT_g/14 judges the similarity between the upper left and upper right panel in Fig. 3 to be more than that between the top right and the bottom right, i.e., 0.94 and 0.88 cosine similarity, respectively. This finding is interesting, given that the covered colored area is similarly large for the two samples indented to 15 nm.

Figuratively speaking, the human eye can clearly identify the top left panel as the child and the upper right as its adult, rugose version. In contrast, the upper and lower right panels represent two different adults. Conventional order parameters indicating similarities would certainly not be able to detect a greater similarity between child and parent than between different children or different parents. We explore next if modern AI is in a position to achieve that.

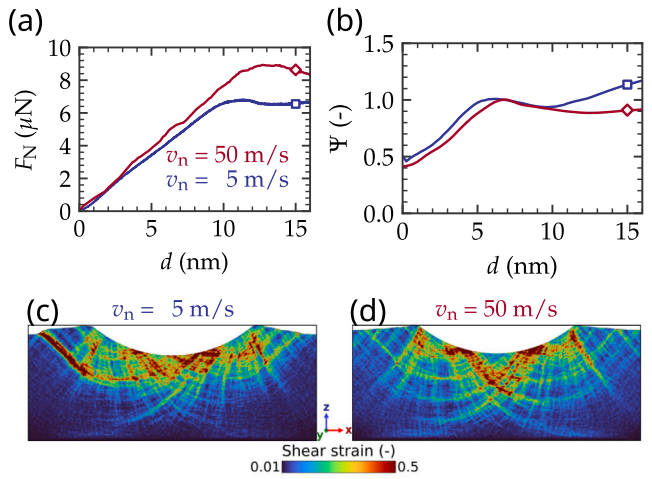

Fig. 5. Contrasting the indentation process of the $T_q = 850$ K fragile glass using two different indentation velocities. Panel (a) shows the normal force F_N and (b) the strain-localization parameter Ψ as a function of displacement d for both velocities. Panel (c) and (d) depict the von Mises shear strain at $d = 15$ nm for $v_0 = 5$ m/s and $v_0 = 50$ m/s, respectively.

Since neither the color maps nor the numbers included in Fig. 6 allow us to conclude whether the two models reveal discontinuities between fragile and strong glasses, a normalized similarity $S_n(T_q)$ of a sample quenched from arbitrary T_q and indented to $d = 15$ nm with that quenched from $T_q = 1{,}000$ K is shown in Fig. 7. It is defined as the normalized cosine similarity between the sample quenched from $T_q = 1000$ K and all other samples at an indentation depth of 15 nm, as defined by

$$S_n(T) = \frac{S_{cos}^{1000\ K}(T) - \min(S_{cos}^{1000\ K}(T_q))}{1 - \min(S_{cos}^{1000\ K}(T_q))}, \quad (1)$$

where $S_{cos}^{T_1}(T_2)$ is the cosine similarity of the flow profiles of quench temperature T_1 and T_2. This measure makes the two studied models operate in a similar domain, because the measure is normalized so that the similarity between the least similar and the $T_q = 1000$ K sample is zero.

Although the similarity indices show a clustering for the strong samples and a jump between strong and fragile samples, the judgment appears less clear than that by humans or the von Mises localization parameter. It is remarkable that both models produce similar results, although the ViT-b/14 has less than 8% of the parameters compared to ViT-g/14.

A final question to be addressed here is to what extent the shape of the flow profiles and shear bands, particularly those obtained for the strong glasses, are erratic or deterministic. All strong samples develop a long shear band to the right with spider-web-like features between the shear band and the surface, plus a shorter but thicker shear band to the left, which is very close to the surface. The probability of breaking the symmetry when quenching from three independent samples each time in the same direction is 1/4, which is small compared to unity but not very small, so it is unclear whether some hidden memory in the strong melt causes the symmetry to break each time in the same direction. We remind the reader that all final configurations share the same ancestor, e.g., the sample obtained after equilibrating the melt at $T = 812$ K was quenched to yield the $T_q = 812$ K glass at 300 K, but also copied and further equilibrated at 800 K for times much exceeding the energy and volume relaxation time.

Since equilibration and indentation simulations require several million CPU hours, averaging over independently produced samples is impractical. To nevertheless ascertain how deterministic features are, we repeated the simulations for a larger cell, in which the quenched samples were not only repeated 14 × 1 × 5 times in x, y, and z-direction, respectively, but 15 × 1 × 6 times (≈ 21.3 Mio). Moreover, the original simulation cell kept its orientation one time but was rotated by 90° so that the original yz surfaces became the new to-be-indented xy surface. Von Mises strains of these three different $T_q = 812$ K samples are contrasted in Fig. 8. The two new configurations show the same characteristics as the old one, i.e., a prominent long shear band, which breaks the symmetry and has the spider-web feature underneath it. Thus, not only the gross but also relatively detailed features of the shear profile appear to be predetermined.

4. Discussion

It is well established that slowly cooling bulk-metallic-glass-forming melts, including their generic in-silico counterparts such as binary Lennard-Jones systems, increases the propensity of the resulting glass to develop localized shear bands [13–15,49]. Moreover, their structure increasingly deviates from the indenter symmetry as the cooling rate decreases [33,49]. A common argument is that a smoother energy landscape, experienced by atoms in a quickly cooled melt, leads to smaller-scale and more homogeneous plastic deformation than that occurring in a slowly cooled glass with a rough energy landscape [15, 50]. However, can this qualitative picture fully show that the strain localization parameter (see Fig. 4) changes only slightly with T_q when T_q is either above or below T^* but so dramatically when passing through the FST?

One potential reason for the discontinuity of the plastic properties could be that the density correlation length ζ in equilibrium melts jumps quasi-discontinuously at T^* [21], whereby the volume of the regions that cooperatively rearrange under shear will also increase. As a consequence, larger energy barriers and, thus, higher stresses need to be overcome to induce plastic flow. This increases the difference between the maximum and the flow stress, whereby strong glasses work-soften substantially more than fragile glasses. This is in line with the fast expansion of STZs into shear bands observed in the strong glasses. As the FST is conjectured to exist in all liquids [21,51–53], we expect similar trends and discontinuities in all glass-forming liquids whose T^* is not too far from T_g.

It remains to be understood what determines the asymmetry of the shear bands and at what point the direction of asymmetry is determined. It seems clear that mature shear bands cannot easily cross because this process would require re-strengthening in the first band or further weakening in the second band, both of which are scarcely energetically favorable. Minor initial asymmetries during the formation of the first STZs appear unavoidable due to the discrete nature of matter and possibly to the finite correlation length of density oscillations. The initial STZs produced in the strong glass show a slightly larger asymmetry parallel to the direction in which the largest mature bands later form. This can be seen in Fig. 9, which contrasts the early STZs in a strong and a fragile sample at an indentation depth of $d = 2.5$ nm, where the strain localization parameter of all samples are essentially identical, which is indicative of a harmonic response. The two snapshots also appear as top-left and second-to-bottom-left panels in Fig. S1, however, with a different color bar. The strong ($T_q = 787$ K) sample forms two STZs with a von Mises strain close to 0.1 about three to four atoms or 6 Å in width parallel to the thin direction. This is on par with $\zeta(T = 787\ K) \approx 5.8$ Å at that temperature, which corroborates a potential link between the liquid structure and the plasticity of the resulting glass. Even during these early stages and long before the formation of mature shear bands, the symmetry breaking in the strong sample is higher than in the fragile one. We note that the two red zones, located to the right of the symmetry axis a little more than 10 nm below the surface in the strong glass, are the seed for a thin shear band that develops during the later stages of the indentation process. Specifically, it is the lowest band in the spider-web-like structure on the r.h.s. of the indenter, which appears to predetermine the direction of the later,

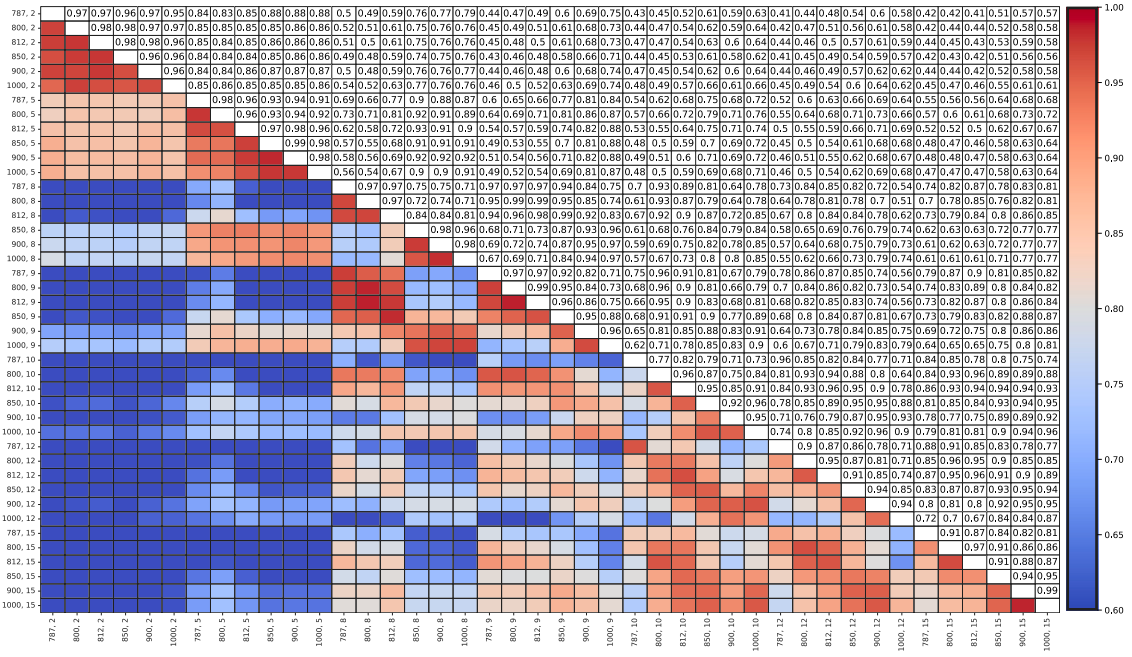

Fig. 6. Cosine similarity matrix using ViTg14 for the images shown in Fig. S1. The first number in each row and column gives T_q in Kelvin, while the second gives d in nm.

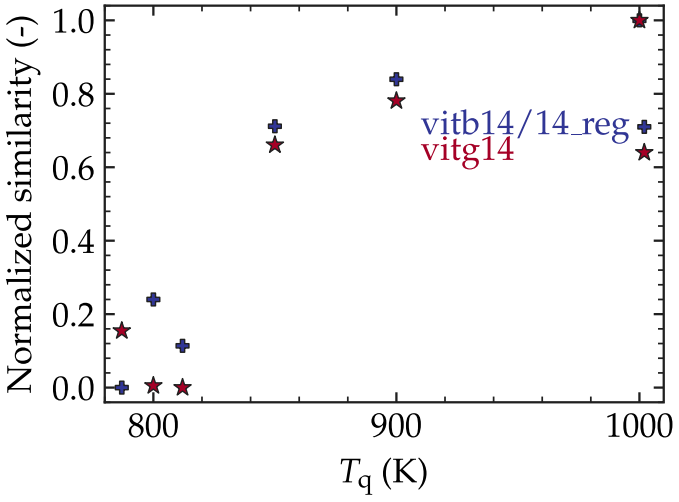

Fig. 7. Normalized similarities measure of a flow profile obtained from a glass quenched from various T_q and from 1 000 K at d = 15 nm for the ViTb/14_reg (plus symbols) and the ViTg/14 (star symbols) models.

much larger mature shear bands beneath it, which are shown in Fig. S1 in the top-right panel. Given the argument at the beginning of this paragraph, the enhanced shear-softening in the strong sample favors the parallel alignment of STZs in them so that a small initial shear band in a strong or shear-softening glass can indeed prescribe the direction of later and larger shear bands.

5. Conclusions

In this paper, we used large-scale molecular dynamics simulations to explore how the fragility of the melt affects the brittleness of BMGs. We showed that melts quenched from just below and above the fragile-to-strong transition temperature show qualitatively different plasticity. The strong glasses exhibit highly localized and strongly asymmetric shear bands. In contrast, the fragile glasses form broader and less defined shear bands. These differences between the strong and the fragile glasses could be easily quantified using a strain localization parameter and pre-trained artificial intelligence models for image similarity.

Our simulations appear to be the first to produce shear-band thicknesses of 8 nm, closely approaching the 10 nm observed experimentally [47]. They may represent the most striking resemblance between in-silico and experimental shear bands reported so far. One reason why we could produce such thick shear bands may be that our system sizes were unusually large (around 20 Mio atoms), and the used potentials are realistic. Equally or more importantly, our glasses could be clearly classified as fragile or strong, whereas glasses in previous simulations were likely a mix of frozen-in fragile and strong liquid structures. Previous recent key contributions using large samples (30 Mio atoms) but generic Lennard-Jones potentials [43] or realistic potentials but smaller sizes (about 0.5 Mio atoms) [45] lead to comparatively thin shear bands of around 3 nm. The glasses indented in those previous simulations were likely strong enough to break the symmetry but too fragile to develop 8 nm thick shear bands.

The observation that strong glasses exhibit more asymmetric and more localized shear bands than fragile glasses is certainly expected. The pioneering simulations by Shi and Falk [14,49] already reproduced the experimental observation that shear bands are more localized and more symmetry broken at lower cooling rates. However, our simulations suggest that this effect is primarily caused by the structural changes a melt undergoes or fails to undergo when passing through the fragile-to-strong transition temperature. This implies that the precise value of the cooling rate used within a sufficient margin of the FST temperature (±20 K would be our rough estimate) should have a relatively minor effect on the mechanical properties of the glass. Last but not least, our simulations reveal that the structure of the shear bands is almost deterministic, except for a mirror inversion, i.e., the direction of symmetry breaking. Not only the shape and location of mature shear bands but also more detailed plastic flow patterns are quite similar between samples that were produced using the same protocol but otherwise consisted of independent initial configurations.

Our findings highlight a potentially overlooked link between the thermodynamic state of the liquid at the FST and the deformation

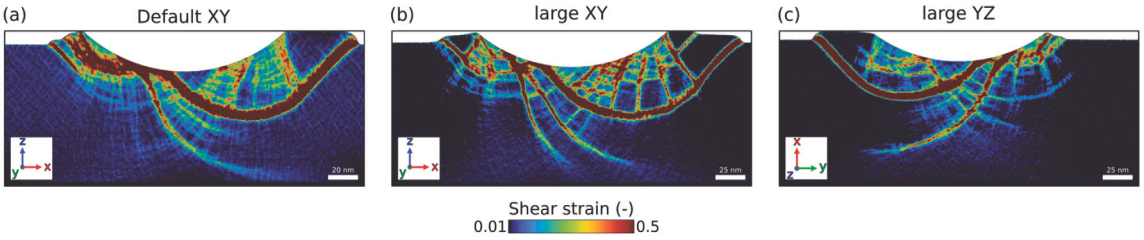

Fig. 8. Von Mises strain of (a) the default set up for T_q = 812 K and a depth of d = 15 nm and (b) and (c) for a slightly larger sample at a depth of d = 15.2 nm. The starting configurations in (b) and (c) differed, i.e., the original glass sample in (c) was rotated by 90° before duplication so that the original yz surface rather than the xy surface was indented.

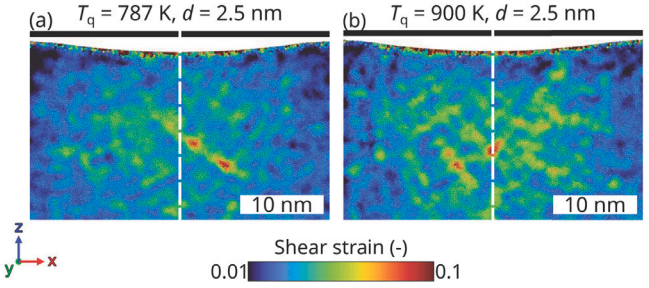

Fig. 9. Von Mises strain maps of (a) strong glass cooled from T_q = 787 K and (b) fragile glass cooled from T_q = 900 K at a depth of d = 2.5 nm. The white dashed line indicates the indenter symmetry axis.

behavior of the resulting glass. This link can be expected to generalize to other classes of glass-forming liquids than BMGs. However, it remains to be determined to what extent the brittleness of other glass-forming systems changes abruptly depending on whether they are cooled from above or below T_{fst}. Perhaps more importantly, it remains to be understood why the relaxation processes occurring in equilibrium in the immediate vicinity of the fragile-to-strong transition have such a dramatic effect on the plasticity of (bulk metallic) glasses, while those outside this domain apparently matter significantly less.

CRediT authorship contribution statement

Achraf Atila: Writing – original draft, Writing – review & editing, Visualization, Resources, Methodology, Investigation, Formal analysis, Conceptualization. **Sergey V. Sukhomlinov:** Writing – review & editing, Resources. **Marc J. Honecker:** Methodology. **Martin H. Müser:** Writing – review & editing, Supervision, Resources, Methodology, Conceptualization.

Declaration of competing interest

The authors declare that they have no known competing financial interests or personal relationships that could have appeared to influence the work reported in this paper.

Acknowledgments

The authors gratefully acknowledge the Gauss Centre for Supercomputing e.V. (www.gauss-centre.eu) for funding this project by providing computing time through the John von Neumann Institute for Computing (NIC) on the GCS Supercomputer JUWELS at Jülich Supercomputing Centre (JSC).

Appendix A. Supplementary data

Supplementary material related to this article can be found online at https://doi.org/10.1016/j.actamat.2025.120753.

References

[1] O. Glushko, R. Pippan, D. Şopu, C. Mitterer, J. Eckert, How to catch a shear band and explain plasticity of metallic glasses with continuum mechanics, Nat. Commun. 15 (1) (2024) http://dx.doi.org/10.1038/s41467-024-49829-2.
[2] A. Inoue, B. Shen, H. Koshiba, H. Kato, A.R. Yavari, Cobalt-based bulk glassy alloy with ultrahigh strength and soft magnetic properties, Nature Mater. 2 (10) (2003) 661–663, http://dx.doi.org/10.1038/nmat982.
[3] R.O. Ritchie, The conflicts between strength and toughness, Nature Mater. 10 (11) (2011) 817–822, http://dx.doi.org/10.1038/nmat3115.
[4] D. Şopu, STZ-vortex model: The key to understand STZ percolation and shear banding in metallic glasses, J. Alloys Compd. 960 (2023) 170585, http://dx.doi.org/10.1016/j.jallcom.2023.170585.
[5] X. Mu, M.R. Chellali, E. Boltynjuk, D. Gunderov, R.Z. Valiev, H. Hahn, C. Kübel, Y. Ivanisenko, L. Velasco, Unveiling the local atomic arrangements in the Shear Band Regions of metallic glass, Adv. Mater. 33 (12) (2021) 2007267, http://dx.doi.org/10.1002/adma.202007267.
[6] Z. Liu, Y. Yang, C. Liu, Yielding and shear banding of metallic glasses, Acta Mater. 61 (16) (2013) 5928–5936, http://dx.doi.org/10.1016/j.actamat.2013.06.025.
[7] C. Packard, C. Schuh, Initiation of shear bands near a stress concentration in metallic glass, Acta Mater. 55 (16) (2007) 5348–5358, http://dx.doi.org/10.1016/j.actamat.2007.05.054.
[8] Z. Xie, D. Chauraud, A. Atila, E. Bitzek, S. Korte-Kerzel, J. Guénolé, Thermally activated nature of synchro-Shockley dislocations in Laves phases, Scr. Mater. 235 (2023) 115588, http://dx.doi.org/10.1016/j.scriptamat.2023.115588, URL https://www.sciencedirect.com/science/article/pii/S1359646223003123.
[9] Z. Xie, D. Chauraud, A. Atila, E. Bitzek, S. Korte-Kerzel, J. Guénolé, Unveiling the mechanisms of motion of synchro-Shockley dislocations in Laves phases, Phys. Rev. Mater. 7 (2023) 053605, http://dx.doi.org/10.1103/PhysRevMaterials.7.053605, URL https://link.aps.org/doi/10.1103/PhysRevMaterials.7.053605.
[10] A. Atila, M. Kbirou, S. Ouaskit, A. Hasnaoui, On the presence of nanoscale heterogeneity in $Al_{70}Ni_{15}Co_{15}$ metallic glass under pressure, J. Non-Cryst. Solids 550 (2020) 120381, http://dx.doi.org/10.1016/j.jnoncrysol.2020.120381.
[11] D. Şopu, S. Scudino, X. Bian, C. Gammer, J. Eckert, Atomic-scale origin of shear band multiplication in heterogeneous metallic glasses, Scr. Mater. 178 (2020) 57–61, http://dx.doi.org/10.1016/j.scriptamat.2019.11.006.
[12] S. Walley, Shear localization: A historical overview, Metall. Mater. Trans. A 38 (11) (2007) 2629–2654, http://dx.doi.org/10.1007/s11661-007-9271-x.
[13] H. Yang, L. Zhang, J. Zhang, H. Tang, S. Chen, Effect of sample size and cooling rate on the plastic deformation behavior of bulk metallic glasses: A comparative study, J. Non-Cryst. Solids 589 (2022) 121643, http://dx.doi.org/10.1016/j.jnoncrysol.2022.121643.
[14] Y. Shi, M.L. Falk, Stress-induced structural transformation and shear banding during simulated nanoindentation of a metallic glass, Acta Mater. 55 (13) (2007) 4317–4324, http://dx.doi.org/10.1016/j.actamat.2007.03.029.
[15] Z. Zhang, J. Ding, E. Ma, Shear transformations in metallic glasses without excessive and predefinable defects, Proc. Natl. Acad. Sci. 119 (48) (2022) http://dx.doi.org/10.1073/pnas.2213941119.
[16] M. Ashby, A. Greer, Metallic glasses as structural materials, Scr. Mater. 54 (3) (2006) 321–326, http://dx.doi.org/10.1016/j.scriptamat.2005.09.051, Viewpoint set no: 37. On mechanical behavior of metallic glasses, URL https://www.sciencedirect.com/science/article/pii/S1359646205006111.

[17] C. Angell, Relaxation in liquids, polymers and plastic crystals — strong/fragile patterns and problems, J. Non-Cryst. Solids 131–133 (1991) 13–31, http://dx.doi.org/10.1016/0022-3093(91)90266-9.

[18] C.A. Angell, Formation of glasses from liquids and biopolymers, Science 267 (5206) (1995) 1924–1935, http://dx.doi.org/10.1126/science.267.5206.1924.

[19] C.A. Angell, K.L. Ngai, G.B. McKenna, P.F. McMillan, S.W. Martin, Relaxation in glassforming liquids and amorphous solids, J. Appl. Phys. 88 (6) (2000) 3113–3157, http://dx.doi.org/10.1063/1.1286035.

[20] M. Stolpe, I. Jonas, S. Wei, Z. Evenson, W. Hembree, F. Yang, A. Meyer, R. Busch, Structural changes during a liquid-liquid transition in the deeply undercooled $Zr_{58.5}Cu_{15.6}Ni_{12.8}Al_{10.3}Nb_{2.8}$ bulk metallic glass forming melt, Phys. Rev. B 93 (2016) 014201, http://dx.doi.org/10.1103/PhysRevB.93.014201, URL https://link.aps.org/doi/10.1103/PhysRevB.93.014201.

[21] S.V. Sukhomlinov, M.H. Müser, Quasidiscontinuous change of the density correlation length at the fragile-to-strong transition in a bulk-metallic-glass forming melt, Phys. Rev. Mater. 2 (2018) 115604, http://dx.doi.org/10.1103/PhysRevMaterials.2.115604, URL https://link.aps.org/doi/10.1103/PhysRevMaterials.2.115604.

[22] M. Ghaemi, M. Jafary-Zadeh, K.H. Khoo, H. Gao, Chemical affinity can govern notch-tip brittle-to-ductile transition in metallic glasses, Extreme Mech. Lett. 52 (2022) 101651, http://dx.doi.org/10.1016/j.eml.2022.101651.

[23] M. Jafary-Zadeh, R. Tavakoli, J. Koh, Z. Aitken, Y.-W. Zhang, Effect of chemical composition and affinity on the short- and medium-range order structures and mechanical properties of Zr-Ni-Al metallic glass, J. Non-Cryst. Solids 456 (2017) 68–75, http://dx.doi.org/10.1016/j.jnoncrysol.2016.10.042.

[24] M.S. Daw, M.I. Baskes, Embedded-atom method: Derivation and application to impurities,surfaces,and other defects in metals, Phys. Rev. B 29 (12) (1984) 6443–6453, http://dx.doi.org/10.1103/physrevb.29.6443.

[25] Y.Q. Cheng, E. Ma, H.W. Sheng, Atomic level structure in multicomponent bulk metallic glass, Phys. Rev. Lett. 102 (2009) 245501, http://dx.doi.org/10.1103/PhysRevLett.102.245501, URL https://link.aps.org/doi/10.1103/PhysRevLett.102.245501.

[26] A. Atila, E.M. Ghardi, S. Ouaskit, A. Hasnaoui, Atomistic insights into the impact of charge balancing cations on the structure and properties of aluminosilicate glasses, Phys. Rev. B 100 (14) (2019) http://dx.doi.org/10.1103/physrevb.100.144109.

[27] A. Atila, Y. Ouldhnini, S. Ouaskit, A. Hasnaoui, Atomistic insights into the mixed-alkali effect in phosphosilicate glasses, Phys. Rev. B 105 (13) (2022) http://dx.doi.org/10.1103/physrevb.105.134101.

[28] T. Schneider, E. Stoll, Molecular-dynamics study of a three-dimensional one-component model for distortive phase transitions, Phys. Rev. B 17 (3) (1978) 1302–1322, http://dx.doi.org/10.1103/physrevb.17.1302.

[29] W. Shinoda, M. Shiga, M. Mikami, Rapid estimation of elastic constants by molecular dynamics simulation under constant stress, Phys. Rev. B 69 (2004) 134103, http://dx.doi.org/10.1103/PhysRevB.69.134103, URL https://link.aps.org/doi/10.1103/PhysRevB.69.134103.

[30] A.P. Thompson, H.M. Aktulga, R. Berger, D.S. Bolintineanu, W.M. Brown, P.S. Crozier, P.J. in 't Veld, A. Kohlmeyer, S.G. Moore, T.D. Nguyen, R. Shan, M.J. Stevens, J. Tranchida, C. Trott, S.J. Plimpton, LAMMPS - a flexible simulation tool for particle-based materials modeling at the atomic, meso, and continuum scales, Comput. Phys. Comm. 271 (2022) 108171, http://dx.doi.org/10.1016/j.cpc.2021.108171, URL https://www.sciencedirect.com/science/article/pii/S0010465521002836.

[31] A. Stukowski, Visualization and analysis of atomistic simulation data with OVITO-the open visualization tool, Model. Simul. Mater. Sci. Eng. 18 (1) (2010) http://dx.doi.org/10.1088/0965-0393/18/1/015012.

[32] E. Lilleodden, J. Zimmerman, S. Foiles, W. Nix, Atomistic simulations of elastic deformation and dislocation nucleation during nanoindentation, J. Mech. Phys. Solids 51 (5) (2003) 901–920, http://dx.doi.org/10.1016/s0022-5096(02)00119-9.

[33] F. Shimizu, S. Ogata, J. Li, Theory of shear banding in metallic glasses and molecular dynamics calculations, Mater. Trans. 48 (11) (2007) 2923–2927, http://dx.doi.org/10.2320/matertrans.mj200769.

[34] M.L. Falk, J.S. Langer, Dynamics of viscoplastic deformation in amorphous solids, Phys. Rev. E 57 (6) (1998) 7192–7205, http://dx.doi.org/10.1103/physreve.57.7192.

[35] M. Oquab, T. Darcet, T. Moutakanni, H.V. Vo, M. Szafraniec, V. Khalidov, P. Fernandez, D. HAZIZA, F. Massa, A. El-Nouby, M. Assran, N. Ballas, W. Galuba, R. Howes, P.-Y. Huang, S.-W. Li, I. Misra, M. Rabbat, V. Sharma, G. Synnaeve, H. Xu, H. Jegou, J. Mairal, P. Labatut, A. Joulin, P. Bojanowski, DINOv2: Learning robust visual features without supervision, Trans. Mach. Learn. Res. (2024) URL https://openreview.net/forum?id=a68SUt6zFt.

[36] A. Dosovitskiy, L. Beyer, A. Kolesnikov, D. Weissenborn, X. Zhai, T. Unterthiner, M. Dehghani, M. Minderer, G. Heigold, S. Gelly, J. Uszkoreit, N. Houlsby, An image is worth 16x16 words: Transformers for image recognition at scale, in: International Conference on Learning Representations, 2021, URL https://openreview.net/forum?id=YicbFdNTTy.

[37] T. Darcet, M. Oquab, J. Mairal, P. Bojanowski, Vision transformers need registers, 2024, arXiv:2309.16588.

[38] A. Paszke, S. Gross, F. Massa, A. Lerer, J. Bradbury, G. Chanan, T. Killeen, Z. Lin, N. Gimelshein, L. Antiga, A. Desmaison, A. Köpf, E. Yang, Z. DeVito, M. Raison, A. Tejani, S. Chilamkurthy, B. Steiner, L. Fang, J. Bai, S. Chintala, PyTorch: An imperative style, high-performance deep learning library, 2019, arXiv:1912.01703.

[39] O. Russakovsky, J. Deng, H. Su, J. Krause, S. Satheesh, S. Ma, Z. Huang, A. Karpathy, A. Khosla, M. Bernstein, A.C. Berg, L. Fei-Fei, ImageNet large scale visual recognition challenge, 2015, arXiv:1409.0575.

[40] S.V. Sukhomlinov, M.H. Müser, Anomalous system-size dependence of properties at the fragile-to-strong transition in a bulk-metallic-glass forming melt, Comput. Mater. Sci. 156 (2019) 129–134, http://dx.doi.org/10.1016/j.commatsci.2018.09.047.

[41] M. Hassani, A.E. Lagogianni, F. Varnik, Probing the degree of heterogeneity within a shear band of a model glass, Phys. Rev. Lett. 123 (2019) 195502, http://dx.doi.org/10.1103/PhysRevLett.123.195502, URL https://link.aps.org/doi/10.1103/PhysRevLett.123.195502.

[42] A. Greer, Y. Cheng, E. Ma, Shear bands in metallic glasses, Mater. Sci. Eng. R 74 (4) (2013) 71–132, http://dx.doi.org/10.1016/j.mser.2013.04.001.

[43] Y. Yang, J. Luo, L. Huang, G. Hu, K.D. Vargheese, Y. Shi, J.C. Mauro, Crack initiation in metallic glasses under nanoindentation, Acta Mater. 115 (2016) 413–422, http://dx.doi.org/10.1016/j.actamat.2016.06.001.

[44] O. Adjaoud, K. Albe, Nanoindentation of nanoglasses tested by molecular dynamics simulations: Influence of structural relaxation and chemical segregation on the mechanical response, Front. Mater. 8 (2021) http://dx.doi.org/10.3389/fmats.2021.664220.

[45] D. Zhao, B. Zhu, S. Wang, Y. Niu, L. Xu, H. Zhao, Effects of pre-strain on the nanoindentation behaviors of metallic glass studied by molecular dynamics simulations, Comput. Mater. Sci. 186 (2021) 110073, http://dx.doi.org/10.1016/j.commatsci.2020.110073.

[46] H. Sheng, D. Şopu, S. Fellner, J. Eckert, C. Gammer, Mapping shear bands in metallic glasses: From atomic structure to bulk dynamics, Phys. Rev. Lett. 128 (24) (2022) http://dx.doi.org/10.1103/physrevlett.128.245501.

[47] Y. Zhang, A.L. Greer, Thickness of shear bands in metallic glasses, Appl. Phys. Lett. 89 (7) (2006) 071907, http://dx.doi.org/10.1063/1.2336598.

[48] Y. Cheng, A. Cao, E. Ma, Correlation between the elastic modulus and the intrinsic plastic behavior of metallic glasses: The roles of atomic configuration and alloy composition, Acta Mater. 57 (11) (2009) 3253–3267, http://dx.doi.org/10.1016/j.actamat.2009.03.027.

[49] Y. Shi, M.L. Falk, Simulations of nanoindentation in a thin amorphous metal film, Thin Solid Films 515 (6) (2007) 3179–3182, http://dx.doi.org/10.1016/j.tsf.2006.01.032.

[50] L. Tang, H. Liu, G. Ma, T. Du, N. Mousseau, W. Zhou, M. Bauchy, The energy landscape governs ductility in disordered materials, Mater. Horiz. 8 (4) (2021) 1242–1252, http://dx.doi.org/10.1039/d0mh00980f.

[51] K. Ito, C.T. Moynihan, C.A. Angell, Thermodynamic determination of fragility in liquids and a fragile-to-strong liquid transition in water, Nature 398 (6727) (1999) 492–495, http://dx.doi.org/10.1038/19042.

[52] P. Lucas, Fragile-to-strong transitions in glass forming liquids, J. Non-Cryst. Solids X 4 (2019) 100034, http://dx.doi.org/10.1016/j.nocx.2019.100034.

[53] Z. Yu, D. Morgan, M.D. Ediger, B. Wang, Understanding the fragile-to-strong transition in silica from microscopic dynamics, Phys. Rev. Lett. 129 (1) (2022) http://dx.doi.org/10.1103/physrevlett.129.018003.